International Journal of Biological Macromolecules 165 (2020) 3078–3087

Contents lists available at ScienceDirect

International Journal of Biological Macromolecules

journal homepage: http://www.elsevier.com/locate/ijbiomac

Fabrication of lignin/poly(3-hydroxybutyrate) nanocomposites with enhanced properties via a Pickering emulsion approach

Ishaq Lugoloobi [a,b], Xiang Li [a], Yunchong Zhang [a,c], Zhiping Mao [a], Bijia Wang [a], Xiaofeng Sui [a,*], Xueling Feng [a,b,**]

[a] Key Lab of Science and Technology of Eco-textile, Ministry of Education, College of Chemistry, Chemical Engineering and Biotechnology, Donghua University, Shanghai 201620, People's Republic of China
[b] National Engineering Research Center for Dyeing and Finishing of Textiles, Donghua University, 10 Shanghai 201620, People's Republic of China
[c] Materials Science and Technology of Polymers, MESA+ Institute of Nanotechnology, University of Twente, P.O. Box 217, 7500 AE Enschede, the Netherlands

ARTICLE INFO

Article history:
Received 10 August 2020
Received in revised form 16 October 2020
Accepted 20 October 2020
Available online 24 October 2020

Keywords:
Particle-reinforcement
PHB
Dispersion
Lignin

ABSTRACT

The present-day world still demands for various commercially viable biosourced materials to replace the finite petroleum-derived polymers. Herein, lignin nanoparticles were homogeneously dispersed in the poly(3-hydroxybutyrate) (PHB) matrix via an economical, simple and environmentally friendly oil-in-water Pickering emulsion approach to form a nanocomposite with improved properties. The prepared lignin/PHB nanocomposites were investigated for their morphological, thermal, optical, rheological and mechanical properties. The lignin nanoparticles proved to be efficient nucleating agents for PHB in that they noticeably increased the crystallization rates of the polymer. PHB film containing 7% lignin demonstrated the optimum improvement in the tensile performance with 13.2% and 43.9% increase in tensile strength and Young's modulus, respectively. This upturn was ascribed to the uniform dispersion of the lignin nanoparticles and the formation of strong interfacial adhesion between the filler and the matrix due to hydrogen bonding interactions. Moreover, lower crystallinity, higher glass transition temperature, improved UV resistance/blocking and higher melt viscosity were achieved in the blends. The synergetic advancement in these properties may be of significant importance for the wider application of bio-sourced PHB in the packaging industry.

1. Introduction

Biodegradable polymers such as poly(3-hydroxybutyrate) (PHB), poly(lactic acid) (PLA) and poly(ε-caprolactone) (PCL) have attracted significant interest both in industry and academia. Among them, PHB is a prominent member in the polyhydroxyalkanoates (PHA) family, it has a good biocompatibility, non-toxicity and complete biodegradability [1]. Though PHB is an excellent candidate for sustainable packaging, its widespread applications are still hindered by some inadequacies such as high costs, high intrinsic fragility [2–4], low and unstable melt strength [5], and low nucleation rates that make the product brittle with occurrence of secondary crystallization [6,7].

Numerous studies have been conducted to improve PHB properties by compositing with various fillers such as natural fibers [8,9], cellulose/starch and their derivatives [10–13], lignin and its derivatives [3,14], pomace extract [15], boron nitride (BN), uracil [16], chitin [17], silica [18], orotic acid (OA) [19], graphene [20], clay, peat, and birchwood flour [21].

In particular, lignin is biodegradable, inexpensive and greatly abundant. It also presents characteristics such as thermal stability, high stiffness [22], antioxidative and UV-blocking properties [23,24]. The preceding research has therefore ascertained that PHB can be blended with different forms of commercial lignin, without modification, to improve its thermal, mechanical, and rheological properties [3,25–28]. Preparation methods such as melt blending [26,29], solvent-assisted casting [14,25,28] and co-rotating twin screw compounding [3,30] have been employed to disperse lignin in PHB. However, the formation of agglomerations and non-uniform dispersion of lignin greatly affect the overall properties of PHB/lignin composites.

Herein, we have employed a Pickering emulsion approach [31–37] to effectively disperse lignin nanoparticles in PHB matrix. The Pickering emulsion approach with lignin stabilizer may result in a more homogeneous dispersion of lignin in the PHB matrix as compared to other methods, leading to improvement of the various properties of PHB. In this work therefore, we present a simple and effective Pickering emulsion method for the preparation of lignin/PHB nanocomposites.

* Corresponding author.
** Correspondence to: X. Feng, Key Lab of Science and Technology of Eco-textile, Ministry of Education, College of Chemistry, Chemical Engineering and Biotechnology, Donghua University, Shanghai 201620, People's Republic of China.
E-mail addresses: suixf@dhu.edu.cn (X. Sui), xlfeng@dhu.edu.cn (X. Feng).

https://doi.org/10.1016/j.ijbiomac.2020.10.156
0141-8130/

Lignin/PHB microparticles were generated by first preparing stabilized Pickering emulsions of PHB and lignin emulsifier in different ratios, followed by solvent evaporation. The microparticles obtained were thereafter molded into films (Scheme 1). The nanocomposites were then characterized for their morphology, thermal, transmittance, mechanical and rheological properties. The morphology-property correlation, focused on enhancement was established to provide an insight to the community of industrial polymer materials for packaging.

2. Experimental parts

2.1. Materials

Poly(3-hydroxybutyrate) (PHB) granules were purchased from Metabolix Ltd. (Mirel M2100, M_n ~ 49,078 Da, M_w ~ 117,869 Da, PDI ~ 2.40). Kraft, alkali lignin powder (AL) with density of 1.3 g/mL at 25 °C, pH 6.5 (25 °C, 5%, aqueous solution) and impurity of 5% moisture, was purchased from Sigma-Aldrich. Ethylene glycol of analytical reagent (AR) grade with ≥99% purity and density of 1.112–1.115 g/mL at 20 °C, was obtained from Shanghai Lingfeng Chemical Reagent Co., Ltd. Phosphoric acid (H_3PO_4, 85% in water) of AR grade was purchased from Shanghai Titan scientific Co., Ltd. Chloroform was purchased from Sinopharm Chemical Reagent Co., Ltd. All reagents were used as received without further purification. Deionized water was used throughout the experiments unless specified.

2.2. Preparation of lignin nanoparticles

The lignin nanoparticles were prepared as reported [36]. In detail, a solution of 4.0 wt% of lignin in ethylene glycol was prepared and magnetically stirred for 3 h at 35 °C. The impurities were removed by vacuum filtration and 800 mL of deionized water was subsequently added. The pH of the lignin solution was adjusted to 2.0 by dropwise addition of H_3PO_4 with continuous stirring. The lignin nanoparticles were obtained by centrifugation and continuous washing with deionized water. The final suspension/dispersion was determined gravimetrically to contain 1.77 wt% of the lignin nanoparticles.

2.3. Preparation of lignin/PHB films

The postulated process for film preparation is demonstrated in Scheme 1. The dispersion of lignin nanoparticles was diluted to 0.125, 0.175 and 0.225 wt% to make lignin/PHB composites of 5, 7 and 9 wt%, respectively. Solution of PHB in chloroform was prepared by dissolving 1 g of PHB granules in 20 mL of chloroform at 40 °C and used as the oil phase. Pickering emulsions with 1:2 (30 mL:60 mL) oil-to-water ratio were prepared by ultrasonication (JY 92-IIDN, 720 W, Scientz, China) for 3 min. The emulsion was set in petri dishes to allow slow evaporation of chloroform at room temperature over 24 h, during which solidified lignin/PHB microparticles were formed. The microparticles were collected by vacuum-filtration and vacuum-dried at 40 °C for 24 h. Finally, blend films were molded by hot compression (Carver-4128, USA) of the lignin/PHB microparticles with 20 MPa pressure at 170 °C for 3 min.

2.4. Sample characterization

2.4.1. Morphological analysis

The morphology of lignin nanoparticles was observed by transmission electron microscopy TEM (JEM-2100, JEOL, Japan) at a voltage of 100 kV. TEM observation was performed on one dried drop of a 0.05% aqueous suspension of lignin nanoparticles on a carbon coated grid (200 mesh).

The morphology of the lignin/PHB microparticles and the surface fracture of their films was studied using scanning electron microscopy (SEM) (TM3030, Hitachi, Japan) and FE-SEM (S-4800, Hitachi, Japan), respectively. The microparticles were spread directly on the conductive adhesive tape. Subsequently, all the samples were coated with a gold-palladium alloy at the thickness of 5 nm, to ensure surface conductivity. The SEM images of the microparticles and films were then obtained.

Optical microscopy ECLIPSE E100 optical microscope (Nikon, Japan) was used to capture the images of the Pickering emulsions at room temperature.

A laser particle-size analyzer (S3500, Microtrac, America) was used to determine the particle size distribution for the lignin/PHB Pickering emulsions at 25 °C by considering six drops for each test. The D50 value was determined by the analyzer as the 50th percentile, and henceforth used to calculate the mean droplet sizes.

2.4.2. Surface elemental analysis

Morphology and surface elemental distribution of neat PHB and the lignin/PHB microparticles were performed by FE-SEM (S-4800, Hitachi, Japan) as described in Section 2.4.1, coupled with an energy dispersive X-ray spectroscope (EDS).

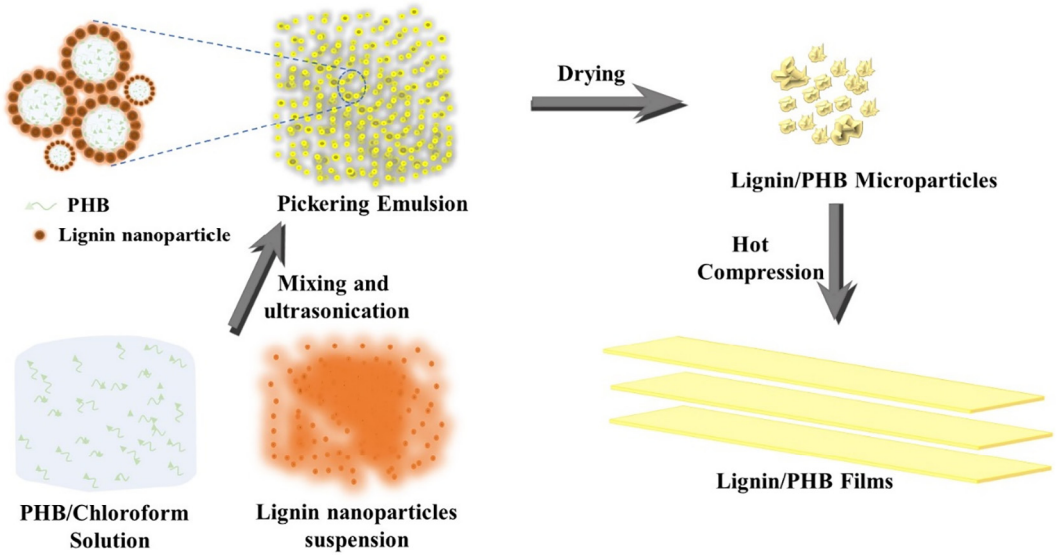

Scheme 1. Schematic illustration showing the preparation of lignin/PHB films via the Pickering emulsion approach.

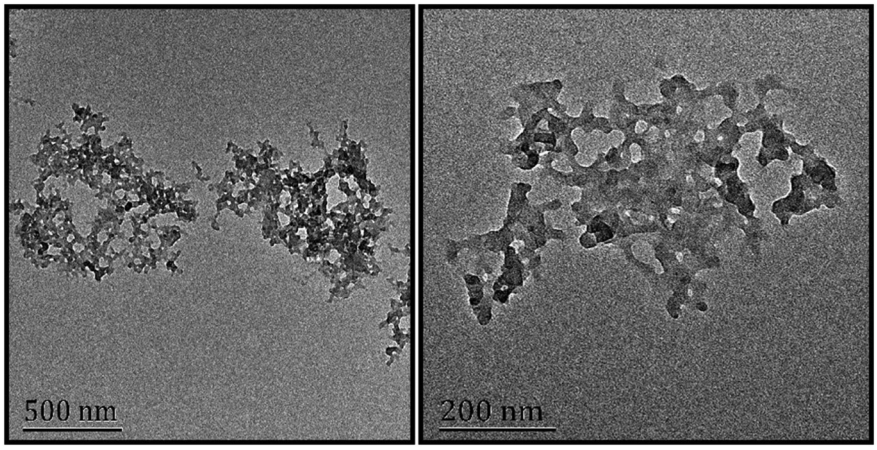

Fig. 1. TEM images of lignin nanoparticles.

2.4.3. Thermal analysis

The decomposition of lignin nanoparticles, neat PHB and lignin/PHB nanocomposite was studied by thermogravimetric analysis (TGA) (209F3, Netzsch, Germany). Under purging of nitrogen, the samples were heated from 30 to 600 °C at a heating rate of 10 °C/min.

The relaxation transition, the melting and crystallization of the samples were investigated using differential scanning calorimetry (DSC) (DSC, 214, NETZSCH, Germany). The samples were heated from −50 to 200 °C, held at 200 °C for 5 min to eliminate thermal history, cooled down to −50 °C, maintained at −50 °C for 5 min and heated again to 200 °C under nitrogen atmosphere. The heating rate was 10 °C/min and the cooling rate was 5 °C/min. Melt crystallization peak temperature (T_{mc}) and crystallization enthalpy (ΔH_{mc}, negative) were determined from the cooling scan. The glass transition temperature (T_g), cold crystallization temperature (T_{cc}), melting temperature (T_m) and melting enthalpy (ΔH_m, positive) were determined from the second heating scan. The crystallinity (χ) of PHB and lignin/PHB nanocomposites was calculated by:

$$X_c(\%) = \left(\frac{\Delta H_m}{\Delta H_m^0}\right) \times 100) \quad (1)$$

where ΔH_m is the experimentally determined melting enthalpy and ΔH°_m is the melting enthalpy of a 100% crystalline PHB (146 J/g) [38].

2.4.4. Ultraviolet–visible spectroscopy

The transmittance of neat PHB and lignin/PHB films (30 μm thick) was measured using a dual-beam ultraviolet–visible (UV–Vis) spectrophotometer (PerkinElmer Lambda 950, USA). The scan was carried out from 250 nm to 800 nm at a high rate.

2.4.5. Tensile properties

The mechanical properties of neat PHB and lignin/PHB films were determined using a universal mechanical testing machine (UH6502, Youhong, China). The gauge length was 50 mm and the testing speed was set to be 10 mm/min. Three parallel measurements were done for each sample.

2.4.6. Rheological properties

Rheological analysis was carried out using a rheometer (Haake-Mars60, Thermo Fisher Scientific, USA) equipped with parallel plates 25 mm in diameter. A frequency sweep from 0.1 to 600 rad/s was used to study the viscoelastic parameters with strain fixed at 1%. The rheological measurements were performed at 175 °C.

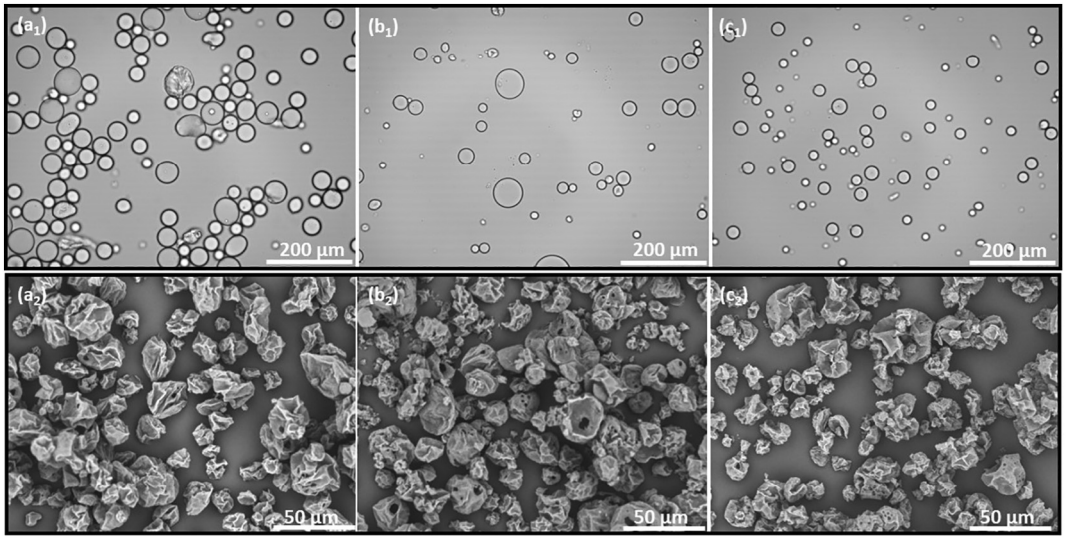

Fig. 2. Optical images of Pickering emulsions stabilized by lignin (above) and SEM images of lignin/PHB microparticles at different concentrations; (a) 5 wt% lignin/PHB, (b) 7 wt% lignin/PHB, and (c) 9 wt% lignin/PHB.

Table 1
Particle diameters of lignin/PHB Pickering emulsions at different lignin concentration.

Sample	Particle diameters (μm)
5% lignin/PHB	52.9 ± 0.5
7% lignin/PHB	46.7 ± 0.4
9% lignin/PHB	39.1 ± 0.5

3. Results and discussions

3.1. Morphological analysis

Lignin nanoparticles were prepared by nanoprecipitation method using ethylene glycol as solvent and their morphology was studied using TEM (Fig. 1). The TEM image of lignin nanoparticles showed symmetrical and roughly spherical nanoparticles interconnected by some glued remaining ethylene glycol solvent, with particle sizes of 30–50 nm.

Optical micrographs of the Pickering emulsions with 5, 7 and 9 wt% ratios and SEM images of the corresponding lignin/PHB nanoparticles are shown in Fig. 2. Emulsions consisted of spherical droplets covered and stabilized with lignin nanoparticles on the surface were formed. The emulsion droplet sizes were obtained using the laser particle size analyzer as the average of the 50th percentile (D50) of emulsion size distribution. For comparison of the three lignin/PHB samples, the emulsion sizes decreased with increasing lignin loading (Table 1). Although a clear shoulder is observed with 7 wt% lignin/PHB emulsions, both 5 wt% and 7 wt% lignin/PHB emulsions displayed monodispersity, while 9 wt% lignin/PHB displayed polydispersity with two peaks at 13.4 ± 0.3 μm and 53.2 ± 1.1 μm (Fig. S1). The second peak was as a result of the large emulsions formed from coalescence of small emulsions, which was partially restrained by the additional lignin nanoparticles adsorbed at the interface. Therefore, 9 wt% lignin/PHB displayed the lowest

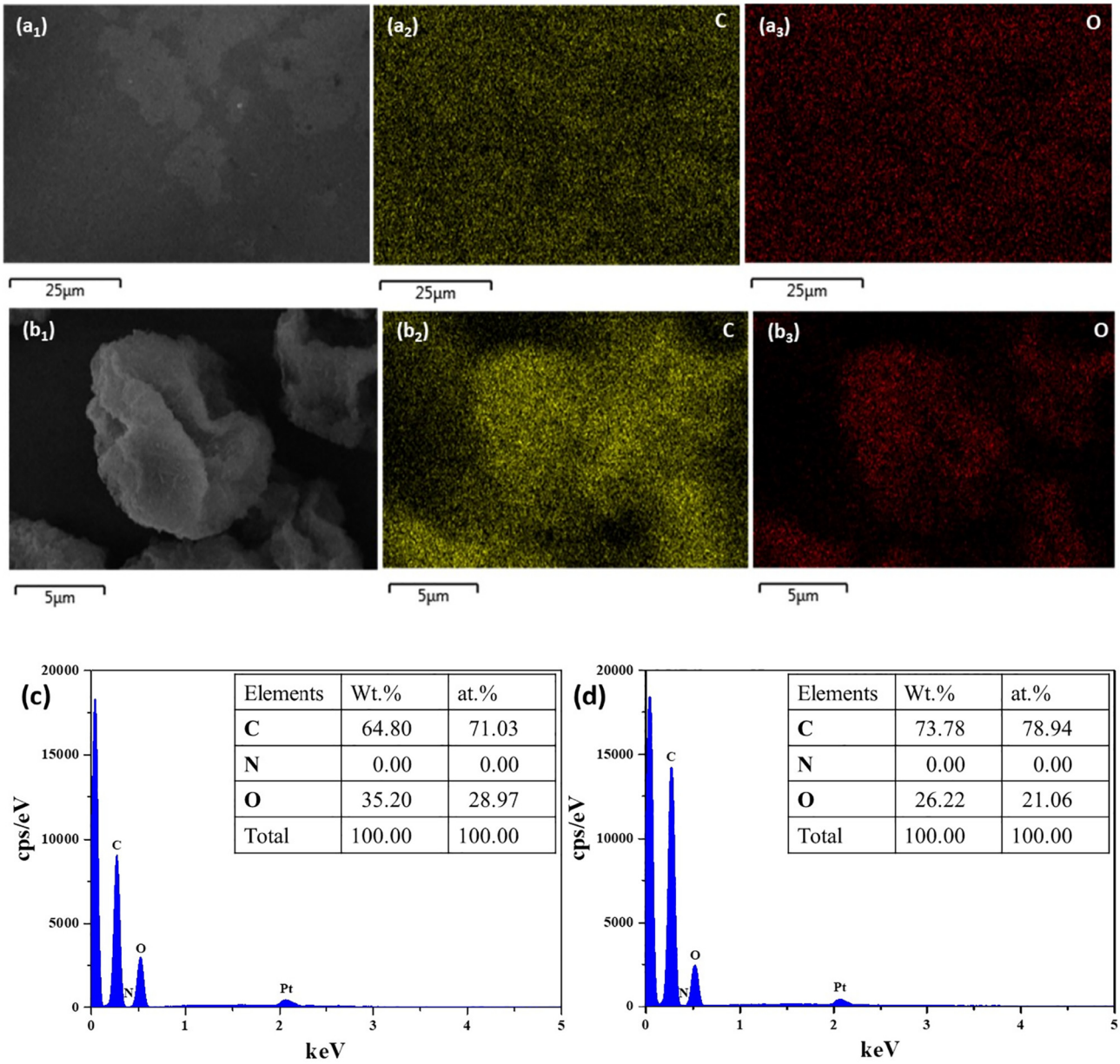

Fig. 3. SEM images ((a_1) and (b_1)) and Elemental distribution on the surfaces of: (a) neat PHB and (b) lignin/PHB microparticles and their EDS spectrum (c) and (d), respectively.

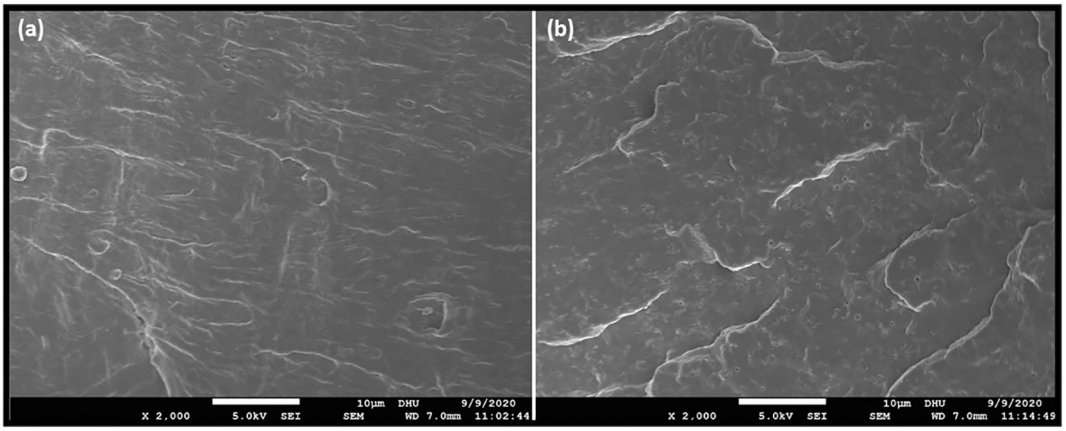

Fig. 4. SEM images of the fracture surface of; (a) neat PHB and (b) lignin/PHB film.

average droplet size (Table 1 & Fig. 2) owed to the high lignin amount. The SEM micrographs showed that all lignin/PHB microparticles were marked with rough, shrunken and porous surfaces and thus, possessing irregular shapes. Powdery microparticles with lignin successfully encapsulated homogeneous within the PHB matrix were obtained.

Fig. 3 shows the C and O elemental contents and distributions on the surfaces of PHB and the lignin/PHB microparticles. The EDS analysis demonstrated that the incorporation of lignin on the PHB surface led to an increase in the carbon content (Fig. 3(c) & (d)), because lignin has a higher carbon content than PHB. Another evidence for the presence of lignin in the composites would be the fact that lignin/PHB microparticles had a yellowish-brown appearance, while neat PHB is white (Fig. S2).

Neat PHB showed a smooth surface whereas the nanocomposite films showed higher degree of surface roughness (Fig. 4). However, the films displayed homogeneous dispersion of lignin within the PHB matrix with no lignin micro agglomerates formed.

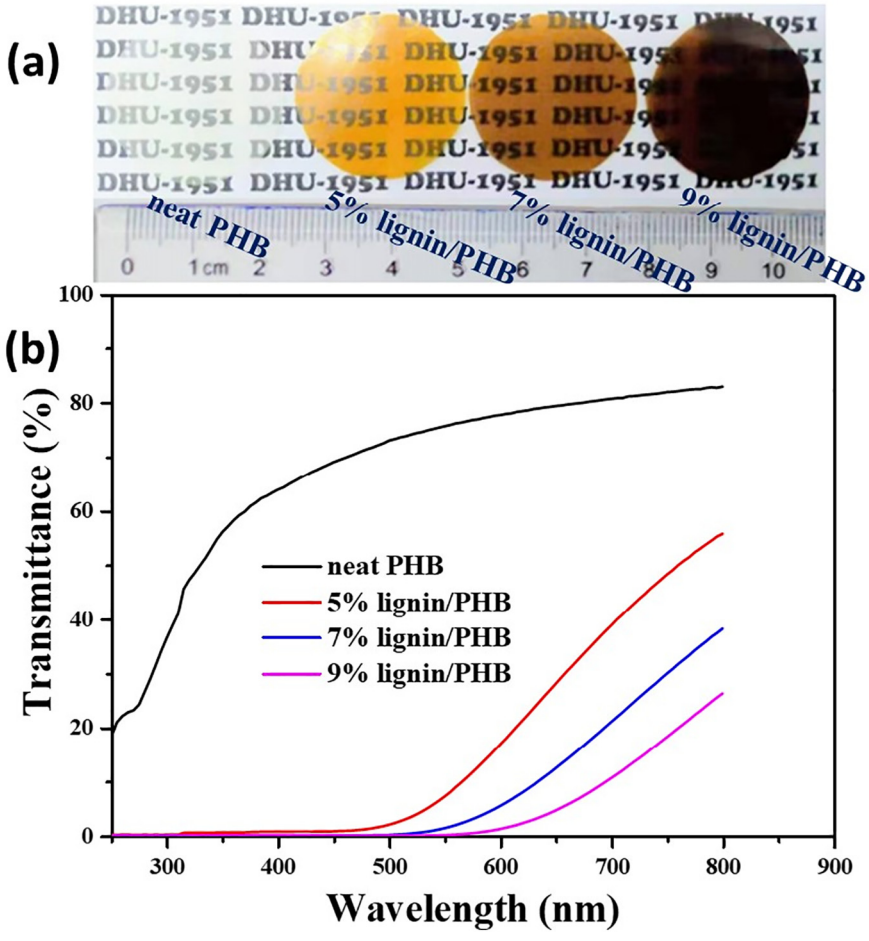

Fig. 5. Photographs (a) and UV–Vis transmission spectra as a function of wavelength (b) of thin films at different lignin concentrations.

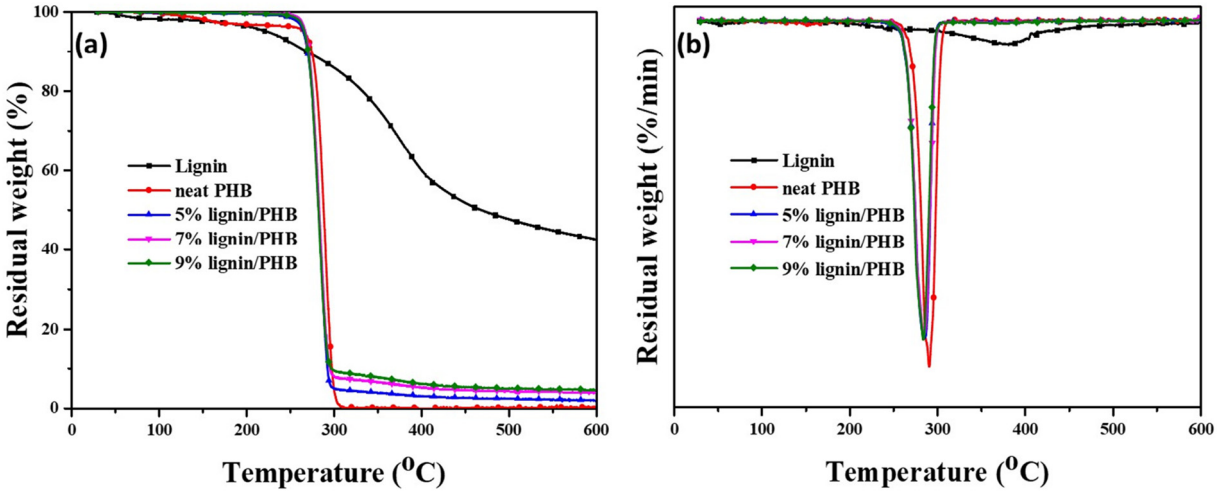

Fig. 6. TGA (a) and DTG (b) traces of lignin, neat PHB and lignin/PHB nanocomposites at different lignin concentrations.

3.2. Optical properties of the composite films

The prepared films were visually examined for their qualitative differences in transparency and external appearance. As shown in Fig. 5 (a), neat PHB is colorless and all lignin/PHB films were colored uniformly due to the presence of lignin nanoparticles, confirming that effective compounding was achieved. The color of the lignin/PHB films appears to be yellowish brown due to their absorption in the blue to violet region of the visible spectrum [39]. The brown color intensified and transparency decreased with increasing lignin content.

The UV–Vis spectra of neat PHB and the lignin/PHB films are presented in Fig. 5(b). Neat PHB displays high transmittance in both visible (400–800 nm) and UV regions (250–400 nm) of the spectrum. In contrast, all the lignin/PHB films display no light transmission in the UV region, demonstrating good UV-blocking properties. These nanocomposite films also strongly absorb in the blue to violet region of the visible spectrum. Fig. 5(b) exhibits some light transmittance of the nanocomposite films in the higher wavelengths of the visible spectrum, however, the intensity decreases with increasing lignin content. This decrease was attributed to the increase in the proportion of dispersed phase in the nanocomposite films that yielded a greater blocking effect probably due to higher refraction and reflection of the projected light [40,41]. It may be also attributed to further absorption in the green region of the visible spectrum with the increase in the lignin particle content.

Table 2
Thermal degradation parameters of neat PHB, lignin/PHB nanocomposites and lignin at different concentrations.

Sample	$T_{o5\%}$	T_{max} (°C)	Char yield (%) at 600 °C
Neat PHB	265.5	291.3	0.3
5% lignin/PHB	265.1	285.2	1.9
7% lignin/PHB	267.5	285.5	4.0
9% lignin/PHB	266.5	284.6	4.6
Lignin	223.1	367.7	42.6

3.3. Thermal behaviors

The thermal stability of the lignin/PHB nanocomposites was studied by TGA and compared to neat PHB and lignin nanoparticles (Fig. 6). The first derivatives of the TGA curves (DTG) are also plotted and compared. Corresponding thermal property data, such as the temperature corresponding to 5 wt% weight loss ($T_{o5\%}$) and char yield/residue (%) at 600 °C, and the maximum degradation rate temperature (T_{max}), were determined and summarized in Table 2. Lignin nanoparticles exhibited

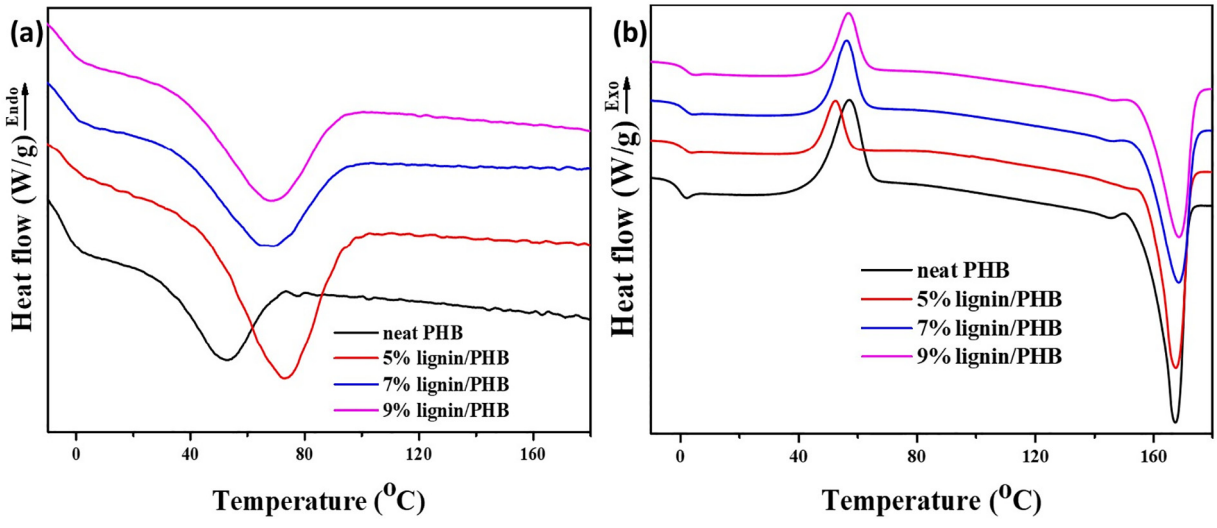

Fig. 7. DSC traces: (a) cooling and (b) second heating scans of PHB and lignin/PHB nanocomposites at different lignin concentrations.

Table 3
DSC analysis of neat PHB and lignin/PHB microparticles from the cooling and second heating scans.

Sample	T_g (°C)	T_{cc} (°C)	T_{mc} (°C)	ΔH_{mc} (J/g)	T_m (°C)	ΔH_m (J/g)	χ (%)
Neat PHB	−1.3 ± 0.4	57.3	53.0	−53.6	167.8 ± 0.1	74.1	50.8
5% lignin/PHB	0.2 ± 0.2	52.7	72.9	−68.2	167.7 ± 0.6	71.3	48.8
7% lignin/PHB	1.3 ± 0.1	56.4	69.3	−59.0	168.6 ± 0.2	65.1	44.6
9% lignin/PHB	2.0 ± 0.1	57.2	68.4	−56.6	169.2 ± 0.5	62.3	42.7

a broad degradation profile, with an initial weight loss below 100 °C due to water evaporation. In detail, lignin degraded slowly from 100 to 270 °C and at a rapid rate from 270 to 460 °C, while portraying the fastest rate at 367.7 °C. The main degradation range was associated with the fragmentation of the inter-unit linkages of lignin, while producing significant amounts of non-volatile solid residue (char yield). Additionally, the DTG curve was less sharp and at a low intensity, portraying a low thermal degradation.

For neat PHB, the first detection was a 4 wt% weight loss at 257 °C, and this was attributed to loss of volatiles due to early depolymerization of PHB. The main degradation step started at 266 °C ($T_{o5\%}$) and the polymer decomposed up to 310 °C, producing very little char. This is ascribed to random chain scission of the polymer caused by higher processing temperatures and longer processing times, and volatilization of the brokendown products. DTG also depicted that T_{max} of neat PHB (291 °C) was slightly higher than T_{max} of the lignin/PHB nanocomposites (Fig. 6(b) & Table 2). Angelini et al [42] reported similar observations and attributed it to lignin that triggered the depolymerization of PHB. High char yield of the lignin/PHB nanocomposites was collected at 600 °C, whose amount increased with increasing lignin content (Table 2), due to the increasing amount of the remaining carbon in lignin.

DSC of neat PHB and the lignin/PHB nanocomposites were compared in Fig. 7. The obtained calorimetric values, including thermal transitions and degree of crystallinity (χ) are listed in Table 3.

During the cooling scans (Fig. 7(a)), neat PHB exhibited a broad exothermic peak with a low intensity and melt crystallization peak temperature (T_{mc}) of 53.0 °C, indicating a rather limited crystallization capability. This could be ascribed to the formation of large sized and low density spherulites that inhibited chain mobility and hindered the crystallization process of the polymer [43]. On the other hand, the crystallization peaks of the lignin/PHB nanocomposites were narrower, sharper and more intense with T_m higher than that of neat PHB (Table 3), suggesting an enhanced tendency towards crystallization. This may have resulted from the nucleation ability of lignin nanoparticles dispersed in PHB, which could promote fast spherulitic growth of numerous low molecular weight PHB chains in the blends. A similar observation was reported in the previous literatures [44,45].

As shown in the second heating thermogram (Fig. 7(b)), the glass transition temperature (T_g) increased from −1.3 °C for neat PHB to 0.2 °C for 5 wt% lignin/PHB nanocomposites (Table 3). This is probably ascribed to the strong interactions between lignin nanoparticles and PHB matrix via hydrogen bonding [46], thus restricting the segmental motion in the polymer chains [45]. It may also be caused by the increase in the crystallization of the amorphous phase of PHB upon cooling. The interactions between lignin nanoparticles and PHB intensified with addition of more lignin nanoparticles of 7 wt% and 9 wt% lignin/PHB (Table 3), leading to further increase in the T_g of the lignin/PHB nanocomposites.

The cold crystallization temperatures (T_{cc}) of lignin/PHB nanocomposites were lower than that of neat PHB while their melt crystallization temperatures (T_{mc}) were higher (Table 3). Usually, T_{mc} and T_{cc} are indirect measures of the crystallization rate, whereby, a lower T_{cc} and a higher T_{mc} indicate faster crystallization [44]. Therefore, the shift of T_{mc} and T_{cc} values of PHB samples to higher and lower temperatures, respectively, indicated that uniform dispersion of lignin in the polymer matrix significantly accelerated its crystallization in both high-temperature and low-temperature regions. As evidenced in Table 3, the variation of T_{mc} and T_{cc} increased with increase of the lignin content in PHB. Camargo et al. [27] attributed this observation to the resistance of the crystallization process of the polymer with the presence of high amounts of lignin. Thus, lignin acted as an effective nucleating agent for PHB.

The degree of crystallinity (χ) of neat PHB and the lignin/PHB nanocomposites was calculated from the melting enthalpy (ΔH_m) (Eq. (1)) [47], as obtained from the second heating scan (Table 3). From Fig. 7 (b), the lignin/PHB nanocomposites have narrow melting ranges and lower melting enthalpies (ΔH_m), and this led to decrease of χ from 50.8% for neat PHB to 48.8% for 5% lignin/PHB and further decrease was observed for nanocomposites containing more lignin content. This could be because the lignin hydroxyl groups and the ester linkages of the polyester segments formed hydrogen bonds that may have altered its chain diffusion and folding during spherulitic growth [48], resulting in a less ordered molecular packing. Higher lignin content in the nanocomposites led to larger number of hydrogen bonding interactions, thus further lowering of crystallinity. The degree of crystallinity (χ) of our lignin/PHB nanocomposites was compared to those of other similar nanocomposites without lignin modification in Table 4. Among all these results, χ of our nanocomposites and that reported by Angelini et al. [25] registered the highest percentage decrease. This portrayed an enhanced tendency towards crystallization with uniform dispersion of lignin in the PHB matrix, via the Pickering emulsion method. However, the melting points (T_m) of PHB were not noticeably changed upon incorporation of lignin. The relaxation behavior from thermal analysis of the nanocomposites (Figs. 6 and 7) can be further studied by Dielectric Relaxation Spectroscopy (DRS) as reported by Ortiz-Serna et al. [49].

Table 4
Degree of crystallinity and tensile properties of lignin/PHB nanocomposites reported in our work and from previous literatures. (LRR refers to Lignin-Rich-Residue, +/− refers to change.)

Ref.	Lignin content in PHB (%)	Percentage decrease in the degree of crystallinity (%)	Percentage change in tensile strength (%)	Percentage change in Young's modulus (%)	Percentage change in elongation at break (%)	Method used
Our work	7	12.2	+13.2	43.9	−28.1	Pickering emulsion
	9	15.9	+12.2	47.9	−45.6	
[3]	20	2.5	–	–	–	Extrusion melt blending
[25]	5 (AL)	16.0	–	–	–	Solvent-assisted blending
	15 (LRR)	3.7	−27.0	−9.7	−40	
[26]	20	7.9	–	–	–	Melt blending
[44]	1	3.2	–	–	–	Manual blending
[50]	25	–	+87.8	–	+112.5	Melt blending

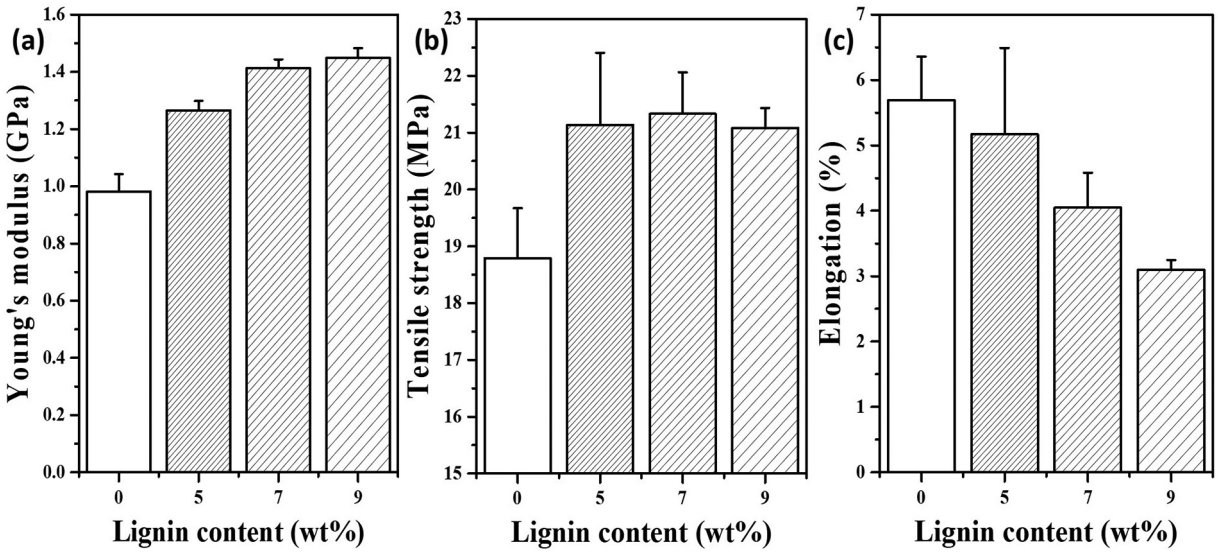

Fig. 8. Tensile property plots of (a) Young's modulus (b) tensile strength and (c) elongation-at-break at different contents of lignin in PHB.

3.4. Tensile properties

Fig. 8 shows the results of Young's modulus, tensile strength and elongation-at-break measurements, which were used to evaluate the mechanical properties of the films reported in this study. Young's modulus increased from 0.98 GPa for neat PHB to 1.45 GPa for 9% lignin/PHB. This increased stiffness of the films with increasing lignin content, was due to the decreased crystallinity of lignin/PHB nanocomposites and stiffness of the lignin phase. The introduction of lignin also resulted in a slight increase in the tensile strength of PHB, from 18.8 MPa for neat PHB to about 21 MPa for the nanocomposite films. Thus, the nanocomposite films virtually showed the same tensile strength (Fig. 8(b)). Most importantly, the tensile strengths of all blend films were higher than that of neat PHB. This enhancement depicted strong interfacial bonding/adhesion between the homogeneously dispersed lignin and PHB matrix, which led to better stress transfer from the soft polymer chains to the stiff lignin. Ren et al [28] also reported a similar observation.

The elongation-at-break decreased from 5.7% for neat PHB to 3.1% for 9% lignin/PHB (Fig. 8(c)), which could be resulted from the enhanced stiffness and decreased segmental mobility of the PHB chains. The presence of the rigid three-dimensional lignin particles may prevent the formation of a long-range continuous phase within the PHB matrix. We also compared the tensile properties of our materials with other lignin/PHB nanocomposites as summarized in Table 4. Singh et al. [50] applied in-situ melt blending process and obtained 87.8% and 112.5% enhancement in the tensile load and elongation at break of nanocomposites prepared from PHB and bagasse lignin. The authors attributed this observation to the lower glass transition temperature of neat PHB than room temperature, leading to crystallization and spherulitic growth of neat PHB, thus, breaks early when stress is applied. However, our nanocomposites expressed higher tensile strength and Young's Modulus compared to those prepared by Angelini et al [25]. This improved mechanical property of our films proves that a continuous mechanical pathway can be formed in the PHB matrix with incorporation of lignin via the Pickering emulsion approach.

3.5. Rheological properties

Fig. 9 depicts the complex viscosity (η^*) and storage modulus (G′) as functions of frequency (ω) of the lignin/PHB blends as compared with neat PHB. In oscillatory shear, η^* is the ratio of shear stress to strain rate amplitudes, which are out of phase for viscoelastic fluids and thus divided into real and imaginary parts [52]. G′ defines the imaginary part of complex viscosity and it measures the energy stored in the

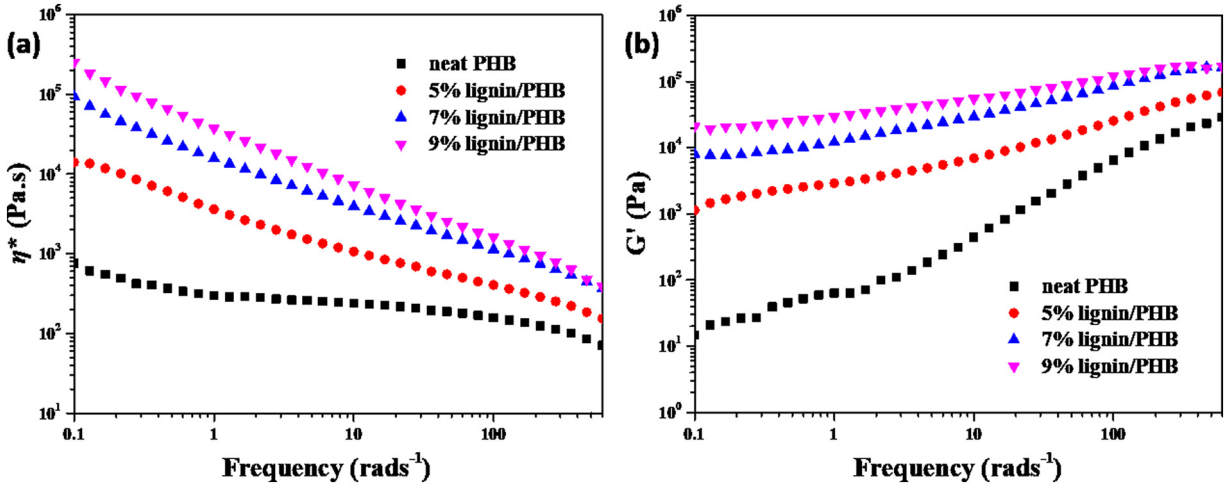

Fig. 9. Complex viscosity (η^*) and storage modulus (G′) of neat PHB and lignin/PHB blend melts at different concentrations with frequency at 175 °C.

material during a half cycle. As shown in Fig. 9, η^* shows opposite trends as a function of frequency to G′. For neat PHB, η^* function portrays a long plateau at frequencies between 1 and 100 rad/s and a slight shear-thinning behavior at frequencies below 1 and above 100 rad/s. While its G′ function presents a typical behavior of molten polymers with a terminal zone of slope of 2 at high frequencies ($\omega > 5$ rad/s). Unlike neat PHB, the η^* curves of the blend films exhibit a shear-thinning behavior without Newtonian plateaus at low frequencies. The G′ curves of the composite films also exhibit a shear-thinning behavior that tends towards a plateau at low frequencies for the 7 and 9 wt% films. The slopes of the G′ curves of the blends were smaller than that of neat PHB at all compositions and independent of frequency (Fig. 9 (b)). These results indicated that the good dispersion of lignin nanoparticles in PHB enhanced their compatibility through hydrogen bond formation. More importantly, both η^* and G′ values of the lignin/PHB blends increased considerably with increasing lignin content at all frequencies, portraying an increasing melt strength (Fig. 9). These results could be attributed to the buildup of a three-dimensional networked structure of lignin nanoparticles joined up by hydrogen bonding, which induced more constraint to chain mobility [53] and led to the transition of the viscoelastic behavior of the PHB melt from liquid-like to solid-like/gel-like behavior. Similar observations were reported in the previous literature [14,52].

4. Conclusion

In this study, we explored the possibility of introducing lignin to improve the performance of PHB. The lignin/PHB nanocomposites were fashioned via a Pickering emulsion approach of PHB and unmodified lignin as a stabilizer, and thereafter hot compressed into films. Lignin successfully improved the crystallization rate of PHB. The lignin/PHB films have no light transmission in the UV region and significantly reduced transmission in the visible region as compared with neat PHB, thus could provide protection against light radiation when used in photoactive packages. Compared to neat PHB film, the Young's modulus and the tensile strength of lignin/PHB films increased, while their elongation-at-break decreased. The blends also displayed a transition from liquid-like to solid-like behavior, hence a widened melt-processing window, due to the buildup of a networked structure inside the polymer matrix. The above enhanced properties suggest that the Pickering emulsion approach was effective in improving the nano dispersion of lignin in PHB matrix, which allows an advantage in various packaging and storage applications..

CRediT authorship contribution statement

Ishaq Lugoloobi: Conceptualization, Investigation, Methodology, Data curation, Formal analysis, Writing - original draft,
Xiang Li: Methodology, Formal analysis, Investigation.
Yunchong Zhang: Formal analysis, Methodology.
Bijia Wang: Conceptualization, Supervision, Writing - review and editing,
Zhiping Mao: Funding acquisition, Supervision, Resources.
Xiaofeng Sui: Conceptualization, Supervision, Resources, Funding acquisition,
Xueling Feng Conceptualization, Funding acquisition, Resources, Supervision.

Declaration of competing interest

No conflict of interest exists in the submission of this manuscript, and the manuscript is approved by all authors for publication. The authors declare that the work described was original research that has not been published previously. It is not under consideration for publication elsewhere, in whole or in part.

Acknowledgements

This work was financially supported by the Fundamental Research Funds for the Central Universities (No. 2232019A3-03).

Appendix A. Supplementary data

Supplementary data to this article can be found online at https://doi.org/10.1016/j.ijbiomac.2020.10.156.

References

[1] J.M. Korde, B. Kandasubramanian, Microbiologically extracted poly (hydroxyalkanoates) and its amalgams as therapeutic nano-carriers in anti-tumor therapies, Mater. Sci. Eng. C Mater. Biol. Appl. 111 (2020), 110799, .
[2] E. Bugnicourt, et al., Polyhydroxyalkanoate (PHA): review of synthesis, characteristics, processing and potential applications in packaging, Express Polym Lett 8 (2014) 791–808.
[3] A.A. Vaidya, et al., Integrating softwood biorefinery lignin into polyhydroxybutyrate composites and application in 3D printing, Mater. Today Commun. 19 (2019) 286–296.
[4] S. Philip, T. Keshavarz, I. Roy, Polyhydroxyalkanoates: biodegradable polymers with a range of applications, J. Chem. Technol. Biotechnol. 82 (2007) 233–247.
[5] A. El-Hadi, Development of a Biodegradable Material Based on Poly(3. hydroxybutyrate) PHB, 2002.
[6] H.S. Barud, et al., Bacterial cellulose/poly(3-hydroxybutyrate) composite membranes, Carbohydr. Polym. 83 (3) (2011) 1279–1284.
[7] R. Chandra, R. Rustgi, Biodegradable polymers, Prog. Polym. Sci. 23 (7) (1998) 1273–1335.
[8] N. Graupner, J. Müssig, A comparison of the mechanical characteristics of kenaf and lyocell fibre reinforced poly(lactic acid) (PLA) and poly(3-hydroxybutyrate) (PHB) composites, Compos. A: Appl. Sci. Manuf. 42 (12) (2011) 2010–2019.
[9] M.A. Gunning, et al., Mechanical and biodegradation performance of short natural fibre polyhydroxybutyrate composites, Polym. Test. 32 (8) (2013) 1603–1611.
[10] M. Zhang, N.L. Thomas, Preparation and properties of polyhydroxybutyrate blended with different types of starch, J. Appl. Polym. Sci. 116 (2) (2010) 688–694.
[11] M. Yamaguchi, K. Arakawa, Control of structure and mechanical properties for binary blends of poly(3-hydroxybutyrate) and cellulose derivative, J. Appl. Polym. Sci. 103 (2007) 3447–3452.
[12] P. Xu, et al., Interfacial modification on polyhydroxyalkanoates/starch blend by grafting in-situ, Carbohydr. Polym. 174 (2017) 716–722.
[13] J.P. Florez, M. Fazeli, R.A. Simao, Preparation and characterization of thermoplastic starch composite reinforced by plasma-treated poly (hydroxybutyrate) PHB, Int. J. Biol. Macromol. 123 (2019) 609–621.
[14] S. Angelini, et al., Acid-insoluble lignin and holocellulose from a lignocellulosic biowaste: bio-fillers in poly(3-hydroxybutyrate), Eur. Polym. J. 76 (2016) 63–76.
[15] P. Persico, et al., Enhancement of poly(3-hydroxybutyrate) thermal and processing stability using a bio-waste derived additive, Int. J. Biol. Macromol. 51 (5) (2012) 1151–1158.
[16] X.-M. Che, H.-M. Ye, G.-Q. Chen, Effects of uracil on crystallization and rheological property of poly(R-3-hydroxybutyrate-co-4-hydroxybutyrate), Compos. A: Appl. Sci. Manuf. 109 (2018) 141–150.
[17] Khasanah, et al., Intermolecular hydrogen bondings in the poly(3-hydroxybutyrate) and chitin blends: their effects on the crystallization behavior and crystal structure of poly(3-hydroxybutyrate). Polymer, 2015. 75: p. 141–150.
[18] P. Maiti, C.A. Batt, E.P. Giannelis, New biodegradable polyhydroxybutyrate/layered silicate nanocomposites, Biomacromolecules 8 (11) (2007) 3393–3400.
[19] Y. Yu, et al., Enhancement of the properties of biosourced poly(3-hydroxybutyrate-co-4-hydroxybutyrate) by the incorporation of natural orotic acid, Int. J. Biol. Macromol. 136 (2019) 764–773.
[20] N.A. Manikandan, K. Pakshirajan, G. Pugazhenthi, Preparation and characterization of environmentally safe and highly biodegradable microbial polyhydroxybutyrate (PHB) based graphene nanocomposites for potential food packaging applications, Int. J. Biol. Macromol. 154 (2020) 866–877.
[21] S. Thomas, et al., Thermal, mechanical and biodegradation studies of biofiller based poly-3-hydroxybutyrate biocomposites, Int. J. Biol. Macromol. 155 (2020) 1373–1384.
[22] Y. Nordström, et al., A new softening agent for melt spinning of softwood kraft lignin, J. Appl. Polym. Sci. 129 (3) (2013) 1274–1279.
[23] D. Kai, et al., New dual functional PHB-grafted lignin copolymer: synthesis, mechanical properties, and biocompatibility studies, ACS Appl. Bio Mater. 2 (1) (2019) 127–134.
[24] A. Naseem, et al., Lignin-derivatives based polymers, blends and composites: a review, Int. J. Biol. Macromol. 93 (Pt A) (2016) 296–313.
[25] S. Angelini, et al., From biowaste to bioresource: effect of a lignocellulosic filler on the properties of poly(3-hydroxybutyrate), Int. J. Biol. Macromol. 71 (2014) 163–173.
[26] P. Mousavioun, P.J. Halley, W.O.S. Doherty, Thermophysical properties and rheology of PHB/lignin blends, Ind. Crop. Prod. 50 (2013) 270–275.
[27] F. Camargo, et al., Processing and characterization of composites of poly(3-hydroxybutyrate-co-hydroxyvalerate) and lignin from sugar cane bagasse, J. Compos. Mater. 46 (2012) 417–425.
[28] S. Qian, X. Dai, Y. Qi, H. Ren, Preparation and characterization of polyhydroxybutyrate-bamboo lignophenol biocomposite films, BioResource 10 (2) (2015) 3169–3180.

[29] E.L. Sánchez-Safont, et al., Biocomposites of different lignocellulosic wastes for sustainable food packaging applications, Compos. Part B 145 (2018) 215–225.
[30] K. Reis, et al., Particles of coffee wastes as reinforcement in polyhydroxybutyrate (PHB) based composites, Mater. Res. 18 (2015).
[31] X. Li, et al., Antibacterial phase change microcapsules obtained with lignin as the Pickering stabilizer and the reducing agent for silver, Int. J. Biol. Macromol. 144 (2020) 624–631.
[32] F.X. Munyazesa, et al., Pickering emulsion process assisted construction of regenerated chitin reinforced poly (lactic acid) blends, Int. J. Biol. Macromol. 140 (2019) 10–16.
[33] L. Rong, et al., Antibacterial thyme oil-loaded organo-hydrogels utilizing cellulose acetoacetate as reactive polymer emulsifier, Int. J. Biol. Macromol. 147 (2020).
[34] Y. Wang, et al., Lignin assisted Pickering emulsion polymerization to microencapsulate 1-tetradecanol for thermal management, Int. J. Biol. Macromol. 146 (2020) 1–8.
[35] Y. Zhang, et al., Poly(lactic acid)/cellulose nanocrystal composites via the Pickering emulsion approach: rheological, thermal and mechanical properties, Int. J. Biol. Macromol. 137 (2019) 197–204.
[36] X. Li, et al., Poly(lactic acid)/lignin blends prepared with the Pickering emulsion template method, Eur. Polym. J. 110 (2019) 378–384.
[37] Y. Jiang, et al., Regenerated cellulose-dispersed polystyrene composites enabled via Pickering emulsion polymerization, Carbohydr. Polym. 223 (2019) 115079.
[38] P.J. Barham, et al., Crystallization and morphology of a bacterial thermoplastic: poly-3-hydroxybutyrate, J. Mater. Sci. 19 (9) (1984) 2781–2794.
[39] T. Simmons, et al., Preparation of synthetic wood composites using ionic liquids, 45 (2010) 719–733.
[40] F. Xiong, et al., Transparent nanocomposite films of lignin nanospheres and poly (vinyl alcohol) for UV-absorbing, Ind. Eng. Chem. Res. 57 (4) (2018) 1207–1212.
[41] W. Yang, et al., Synergic effect of cellulose and lignin nanostructures in PLA based systems for food antibacterial packaging, Eur. Polym. J. 79 (2016) 1–12.
[42] S. Angelini, et al., Extraction and fractionation of a lignocellulosic biomass and its use as a bio-filler in poly(3-hydroxybutyrate), Cellul. Chem. Technol. 50 (2016) 429–437.
[43] A. El-Hadi, et al., Correlation between degree of crystallinity, morphology, glass temperature, mechanical properties and biodegradation of poly (3-hydroxyalkanoate) PHAs and their blends, Polym. Test. 21 (6) (2002) 665–674.
[44] K. Weihua, et al., Effect of lignin particles as a nucleating agent on crystallization of poly(3-hydroxybutyrate), J. Appl. Polym. Sci. 94 (6) (2004) 2466–2474.
[45] S. Luo, J. Cao, A.G. McDonald, Interfacial improvements in a green biopolymer alloy of poly(3-hydroxybutyrate-co-3-hydroxyvalerate) and lignin via in situ reactive extrusion, ACS Sustain. Chem. Eng. 4 (6) (2016) 3465–3476.
[46] B. Podolyák, et al., Hydrogen bonding interactions in poly(ethylene-co-vinyl alcohol)/lignin blends, Int. J. Biol. Macromol. 107 (2018) 1203–1211.
[47] T. Murayama, Dynamic Mechanical Analysis of Polymeric Material, 1978.
[48] H.-Y. Yu, J.-M. Yao, Reinforcing properties of bacterial polyester with different cellulose nanocrystals via modulating hydrogen bonds, Compos. Sci. Technol. 136 (2016) 53–60.
[49] P. Ortiz-Serna, et al., Exploring the role of lignin structure in molecular dynamics of lignin/bio-derived thermoplastic elastomer polyurethane blends, Int. J. Biol. Macromol. 158 (2020) 1369–1379.
[50] P.K. Singh, In situ mixing of polyhydroxybutyrate (PHB) and solvent extracted bagasse lignin, Int. J. Sci. Technol. Eng. 2 (8) (2016) 67–75.
[52] D. Bagheriasl, et al., Shear rheology of polylactide (PLA)–cellulose nanocrystal (CNC) nanocomposites, Cellulose 23 (3) (2016) 1885–1897.
[53] A. Ghanbari, et al., Morphological and rheological properties of PET/clay nanocomposites, Rheol. Acta 52 (1) (2013) 59–74.